

Effects of 2,2-Dichloroacetamide Additive on Perovskite Solar Cells Efficiency

Adem Mutlu^{1*} , Sevdıye Başak Turgut¹ 

¹ Solar Energy Institute, Ege University, Izmir, Türkiye, 35100

* adem.mutlu@ege.edu.tr

* Orcid No: 0000-0002-1696-4379

Received: 9 November, 2024

Accepted: 16 December, 2024

DOI: 10.18466/cbayarfbe.1582175

Abstract

This study investigates the effect of adding 2,2-dichloroacetamide (DCA) to the anti-solvent process in perovskite film fabrication. The results show that DCA additive increases the apparent grain size of the perovskite, reduces crystal defects, and improves the optoelectronic properties of perovskite solar cells (PSCs). Triple-cation perovskite thin films modified with DCA exhibit a 16% improvement in device performance compared to the unmodified control cell, due to increased emission intensity, longer charge carrier lifetimes, and passivation of surface defects, resulting in reduced hysteresis. The use of DCA reduces charge carrier recombination losses in PSCs, leading to enhancements in fill factor (FF), short-circuit current density (J_{sc}), and power conversion efficiency (PCE), increasing the PCE of the control cell from 12.6% to 14.6%. This research highlights the potential of molecular additives to optimize crystallization kinetics, facilitating the development of more efficient PSCs. The findings reveal that DCA additive plays a significant role in enhancing perovskite film quality. This strategy has the potential to improve the structural integrity and optoelectronic properties of perovskite layers, thereby enhancing the performance of solar cells.

Keywords: perovskite, solar cell, efficiency, crystallization, passivation, anti-solvent, additive

1. Introduction

Perovskite solar cells (PSCs) are widely recognized as a leading and rapidly developing technology in the field of renewable energy. The high production costs and efficiency limitations of traditional silicon-based solar cells have increased the demand for more cost-effective alternatives. On the other hand, PSCs have attracted considerable attention in the photovoltaic industry because of their low production costs, flexible manufacturing processes, and improving efficiency due to continuous research and development. Materials such as methylammonium lead iodide ($\text{CH}_3\text{NH}_3\text{PbI}_3$) in perovskite solar cells are more effective at converting sunlight into electricity, thanks to their wide light absorption spectrum and high charge carrier mobility, thereby enhancing device performance [1-3]. Thanks to these key properties, the efficiency of PSCs has risen from 3.8% to 26.7% through various studies, bringing them close to competing with silicon-based cells [4]. However, one of the biggest challenges faced by perovskite solar cells is their environmental stability,

which is not yet sufficient for long-term use. The perovskite structure is prone to degradation when exposed to factors like thermal stability, moisture, and oxygen. This degradation reduces the material's performance over time and slows down the transition to commercial use [5,6]. The volatility of organic components in the perovskite structure and their sensitivity to environmental factors lead to structural degradation and the formation of unwanted by-products such as lead iodide (PbI_2). Therefore, various strategies are being developed to improve the long-term stability of PSCs [7,8]. Changes in the perovskite structure and composition have been shown to enhance stability by achieving a more crystalline and homogeneous surface and creating larger grain boundaries, which in turn improve the material's stability [9]. One of the most common methods to address stability issues is modifying the chemical composition of the perovskite structure and optimizing the film morphology. For example, replacing methylammonium (MA^+) ions with more stable cations such as cesium (Cs^+) and formamidinium (FA^+) reduces the degradation tendency of the structure and enhances the environmental stability of PSCs. This type of

structure, known as a triple-cation structure, forms the CsFAMA composition. Triple-cation structures offer higher stability and efficiency compared to single-cation ones, making PSCs more resistant to environmental factors. Additionally, using different halogens such as iodide (I⁻), bromine (Br⁻), and chlorine (Cl⁻) in the perovskite material helps broaden the light absorption spectrum and increase charge carrier mobility, enabling the production of more efficient devices. These modifications reduce crystal defects and minimize carrier losses by obtaining larger grain boundaries in the perovskite layer [10-12].

Various approaches have been developed to reduce crystal defects and prevent charge carrier recombination in perovskite films [13-15]. The use of additives is one such effective method. Additives that influence crystal growth and film morphology play a crucial role in obtaining more stable and efficient devices [16,17]. Studies by researchers such as Zhang and Snaith have demonstrated that certain additives can stabilize the structure and enhance the efficiency of PSCs. These additives passivate defects on the crystal surfaces, reducing carrier losses and improving device performance [18,19].

The production processes of perovskite thin films have a significant impact on solar cell performance. Solution-based techniques are commonly used in PSC fabrication, and these techniques directly affect the quality of the perovskite thin films. Solution-based methods like the anti-solvent technique are employed to optimize the crystallization rate and surface morphology of perovskite solutions. However, to achieve stable crystal structures and smooth morphology, the use of additional additives during the anti-solvent process is necessary. Additives incorporated into anti-solvents help regulate the crystallization process, leading to the formation of more stable and efficient structures [9,20,21].

In this study, we focused on incorporating 2,2-dichloroacetamide (DCA) additive into the anti-solvent to improve the crystallization process and surface morphology of perovskite films. By regulating the crystallization kinetics, DCA creates a structure in the film where perovskite crystallization is enhanced and defects are passivated, thereby minimizing carrier losses. The results of the analysis show that DCA directs crystal growth, leading to a smoother and homogeneous surface with higher crystallinity. As a result, the perovskite film's light absorption increases, charge carrier recombination decreases, and the overall optoelectronic performance of the device improves.

2. Materials and Methods

2.1. Materials

The lead iodide (PbI₂, 99.99%) used in the study was obtained from Tokyo Chemical Industry (TCI). 2-

Propanol (HPLC, 99.9%), titanium isopropoxide (Ti[OCH(CH₃)₂]₄, 97%), acetonitrile (anhydrous ACN, 99.8%), hydrochloric acid (HCl, 37%), chlorobenzene (anhydrous CB, 99.8%), cesium iodide (CsI, 99.999%), 4-tert-butylpyridine (4-tBP, 98.0%), and 2,2-dichloroacetamide (DCA) were obtained from Sigma-Aldrich. Fluorine-doped tin oxide glass (FTO) with a sheet resistance of 14 Ohm/sq and dimensions of 2.5x2.5 cm² were provided by OPVTECH (FTO22-15). Lead bromide (PbBr₂, 99.999%), methylammonium bromide (MABr, >99.5%) and formamidinium iodide (FAI, >99.5%) were supplied by Lumtec. Spiro-OMeTAD was purchased from Borun. Anhydrous N,N-dimethylformamide (DMF, >99.5%) and bis(trifluoromethanesulfonyl) lithium salt (Li-TFSI, 99.0%) were provided by Acros, while dimethyl sulfoxide (DMSO, >99.7%) was obtained from Merck.

2.2. Characterization

Various experimental methods and devices were used for the characterization of photovoltaic devices. Electrical properties were determined through current density-voltage (J-V) measurements performed using a Keithley 2400 source meter under AM1.5G simulation, while morphological and structural properties were examined with an Ambios atomic force microscope (AFM) and a Panalytical X-ray diffractometer (XRD). Optical properties were analyzed by obtaining absorption spectra using a Perkin Elmer Lambda 950 UV-Vis spectrophotometer, and photoluminescence (PL) and time-resolved photoluminescence (TRPL) spectra were recorded with an Edinburgh Instruments system under pulsed laser excitation at 655 nm. Fourier Transform Infrared Spectroscopy (FTIR) spectroscopy was performed using a Thermo Scientific Nicolet iS50 device, and film thickness was measured with a Dektak profilometer.

2.3. Device fabrication

FTO substrates, 2.5 cm x 2.5 cm in size, were initially cleaned for 20-minutes using a sequence of distilled water, acetone, and 2-propanol. Titanium dioxide (TiO₂) was synthesized by the sol-gel method. The cleaned FTO glass substrates underwent a 7-minute oxygen plasma treatment, followed by the application of a TiO₂ solution using spin coating at 2000 rpm for 20 seconds to create a uniform layer. Finally, the coated films were annealed at 460°C for 1 hour to achieve the anatase crystal structure of TiO₂. Then, a 0.1 M Li-TFSI solution prepared in anhydrous ACN was applied onto the TiO₂-coated films at 3000 rpm for 40 seconds, followed by another 1 hour annealing at 460°C. To maintain a controlled environment, all coating operations for the subsequent layers were performed inside a glovebox. A triple-cation perovskite solution with the composition of Cs_{0.05}(FA_{0.83}MA_{0.17})_{0.95}Pb(I_{0.83}Br_{0.17})₃ was dissolved in an anhydrous DMF and DMSO (4:1 ratio) mixture [11,22].

The prepared perovskite solution was applied to the Li-TiO₂-coated substrates through a two-step spin-coating process: the first step was performed at 2000 rpm for 25 seconds, followed by the second step at 4000 rpm for 20 seconds. During the second step, the surface was washed with 100 μ L of anhydrous CB at the 10th second. DCA was added to the CB at a concentration of 1 mg/mL. To enhance the solubility of DCA, it was kept in an ultrasonic bath at 50°C for 20 minutes. The anti-solvent process was carried out with both CB (control) and CB+DCA, and the perovskite thin films were annealed at 100°C for 1 hour to achieve a high-quality perovskite structure. Spiro-OMeTAD, was prepared by dissolving it in anhydrous CB at a concentration of 73 mg/mL. To this solution, 30 μ L of 4-tBP and 16 μ L of a Li-TFSI/acetonitrile solution (520 mg/mL) were added to enhance charge transport. The resulting mixture was uniformly deposited onto the substrate using spin coating at 4000 rpm for 20 seconds. To complete the device, a thin film of molybdenum trioxide (MoO₃, 8 nm thick) was thermally evaporated onto the Spiro-OMeTAD layer, followed by a thicker layer of silver (Ag, 100 nm thick). The entire process was carried out under high vacuum conditions (2×10^{-7} Torr). The active area of the devices is 0.095 cm².

3. Results and Discussion

The configuration of the PSCs with the FTO/Li-TiO₂/CsFAMA/Spiro-OMeTAD/MoO₃/Ag is shown in Figure 1a. The triple-cation perovskite thin films were coated using the spin-coating method, aided by an anti-solvent [11]. During the perovskite thin film coating, DCA material was used within the CB anti-solvent to control the crystallization kinetics. The influence of DCA molecules on the perovskite was examined using various techniques, including XRD, AFM, PL, TRPL, UV-Vis spectroscopy, and FTIR spectroscopy. As shown in the XRD patterns in Figure 1b, the diffraction peaks from all perovskites were almost identical. Characteristic peaks associated with the CsFAMA perovskite structure were observed at 2θ values of 14.03°, 20.0°, 24.47°, 28.3°, 31.7°, 34.87°, 40.46°, and 43.0°, consistently appearing in all films treated with either the control or DCA molecules.[23] Notable differences were observed in the peak intensities at $2\theta=14.03^\circ$ and 28.3° , corresponding to the (110) and (220) planes, respectively. Bakr et al. achieved a similar oriented growth using alkylamine ligands (AALs). The films treated with AALs demonstrated enhanced growth along the (110) orientation, showing a reduction in trap state density, as well as improvements in charge mobility and diffusion length [24]. The lack of any change in the peak positions of the perovskite indicates that the perovskite structure is not significantly affected by the DCA molecule used; however, it is understood that these molecules contributed to the oriented growth of the perovskite grain boundaries [25].

The absorption spectra in Figure 2a reveals that all perovskite thin films exhibit similar patterns. Since the perovskite structure is not significantly affected by the DCA molecule, no substantial differences in the bandgap energies are expected. The bandgap energy of the control film, calculated from the Tauc plots, is 1.612 eV, which is consistent with the literature (Figure 2b). [11,26]. For the perovskite sample modified with DCA within the anti-solvent, the bandgap energy was calculated to be 1.606 eV. The average film thicknesses of the perovskite films washed with CB and CB+DCA were found to be 400 ± 5 nm and 450 ± 10 nm, respectively. As the thickness of the perovskite thin films increases, light absorption also increases. Consequently, the film washed with CB+DCA exhibits the highest absorbance [27].

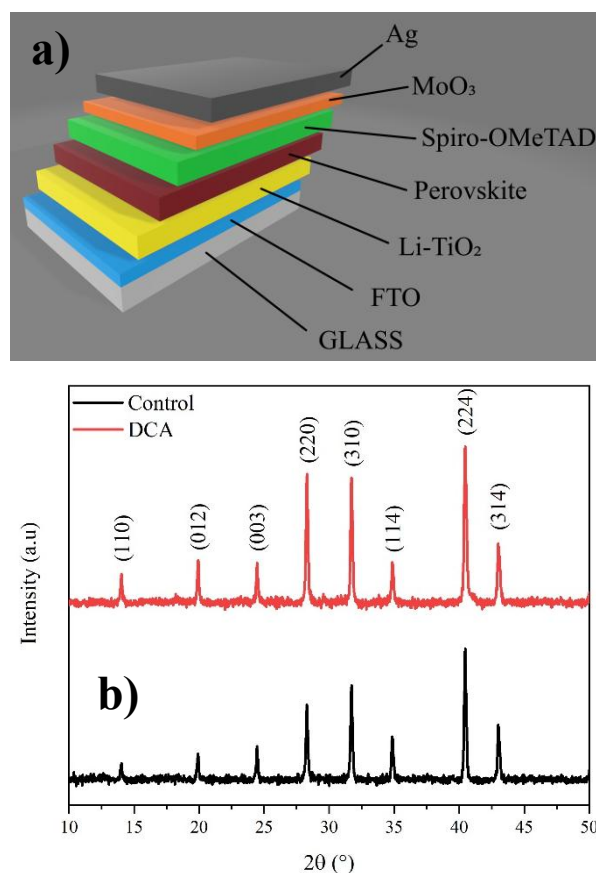


Figure 1. a) Device configuration, b) XRD spectra of control and DCA-modified triple cation perovskite thin films.

Figure 3a displays the PL spectra of perovskite thin films coated on glass substrates with and without the use of DCA molecules in anti-solvent. The PL peak at approximately 770 nm for the reference triple cation perovskite structure aligns with the literature. Notably, the PL intensities of the perovskite film coated with DCA were higher than those of the control film, suggesting that the use of DCA effectively reduces non-radiative recombination in the perovskite layer. Defects in perovskite films serve as trap centers for charge carriers,

leading to energy loss via non-radiative recombination pathways. To investigate the impact of the DCA molecules on the photoluminescence dynamics, TRPL decay measurements were conducted at the primary PL peak of 770 nm, using an excitation laser with a wavelength of 656 nm (Figure 3b). These components allow the extraction of two types of recombination regimes: τ_1 , dominated by interfacial recombination with a short carrier lifetime, and τ_2 , dominated by bulk recombination with a long carrier lifetime [28,29]. The τ_2 value of the DCA-modified perovskite thin film increased from 94.03 ns to 208.53 ns (Table 1). The longer carrier lifetime in the DCA-modified perovskite film indicates a significant reduction in non-radiative recombination of carriers due to the elimination of defects [30].

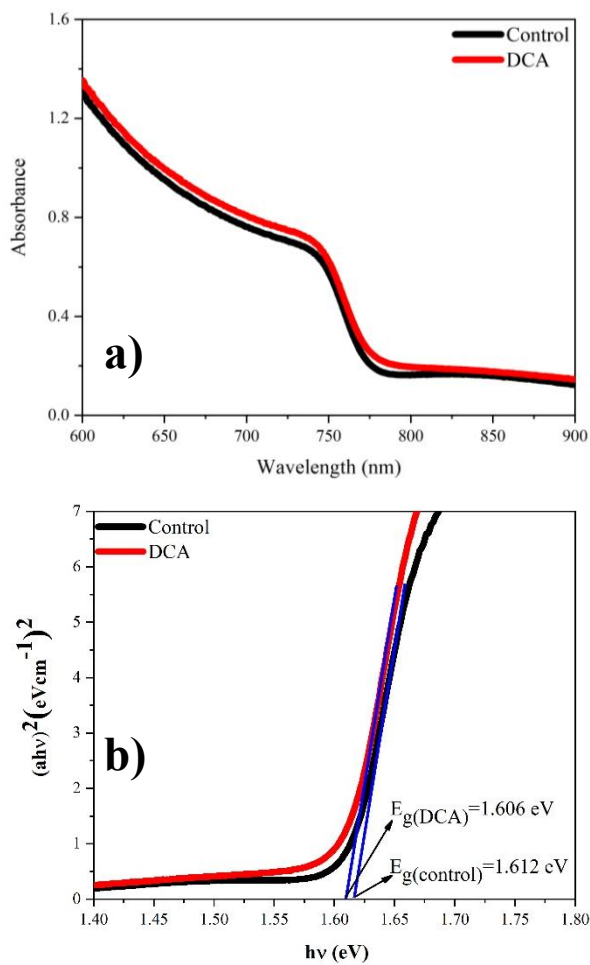


Figure 2. (a) UV-Vis spectra and (b) Tauc plots of control and DCA-modified triple cation perovskite thin films.

Table 1. TRPL parameters of control and DCA-modified perovskite thin films.

ID	τ_1 (ns)	τ_2 (ns)	χ^2
Control	21.44	94.03	1.126
DCA	44.43	208.53	1.179

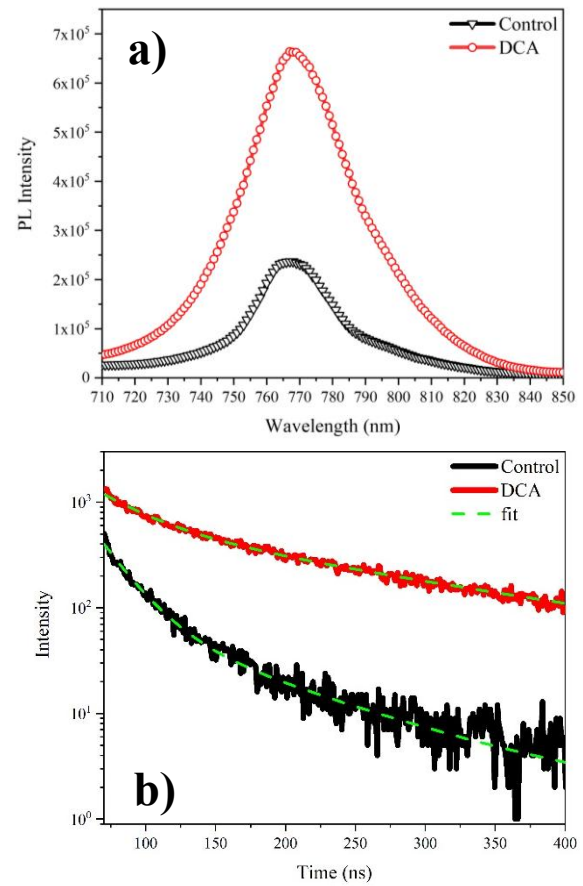


Figure 3. (a) PL and (b) TRPL spectra of control and DCA-modified triple cation perovskite thin films.

FTIR spectra were measured to observe the effect of the DCA molecule within the perovskite structure. To determine the interaction between the C=O bond in the DCA molecule and Pb^{+2} in the perovskite, FTIR spectra of both the control and DCA-modified thin films are presented in Figure 4. In the DCA-modified thin film, the characteristic peak of the C=O bond appears at a wavenumber of 1681 cm^{-1} , which is consistent with the literature [31,32]. The presence of the C=O stretching vibration peak at 1681 cm^{-1} in the film modified with this molecule clearly indicates that DCA has been incorporated into the perovskite film and interacts with Pb^{+2} within the perovskite structure. The electron pair on the oxygen atom of the C=O bond can provide strong coordination with Pb^{+2} , potentially forming nucleation centers around the DCA and supporting the slow and uniform growth of the perovskite layer. As a result of this effect, perovskite crystals grow gradually and evenly around the nucleation centers, forming a high-quality film with large grain size [31].

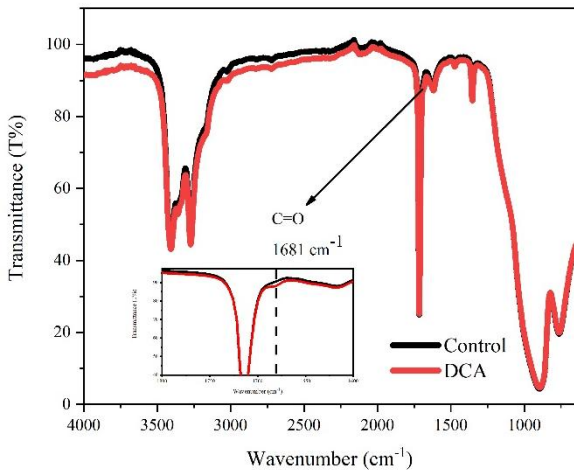


Figure 4. FTIR spectra of DCA-modified and unmodified perovskite thin films.

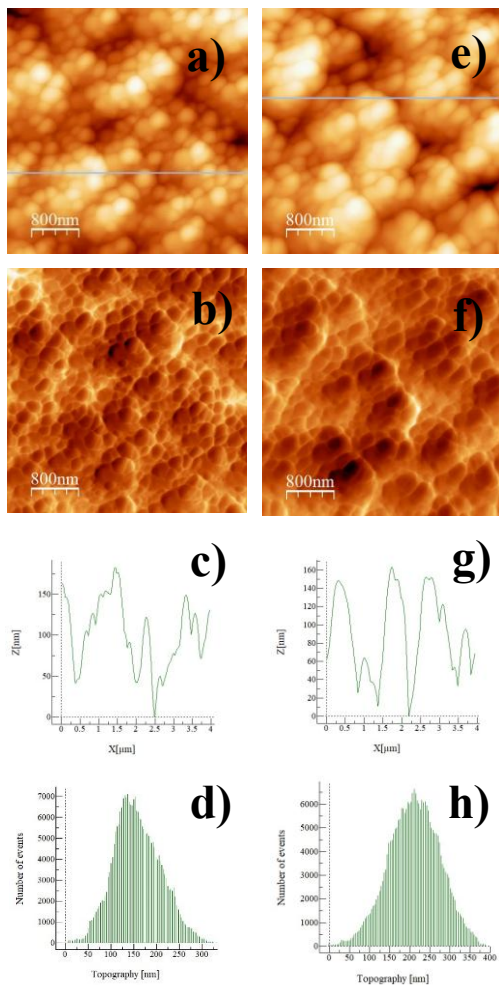


Figure 5. $4 \times 4 \mu\text{m}^2$ AFM images, phase images, profiles, and topographies of control (a-d) and DCA-modified (e-h) perovskite surfaces.

AFM was used to investigate the morphological properties of the perovskite thin films. Figure 5 presents AFM images, phase images, profiles, and topographic images obtained from a $4 \times 4 \mu\text{m}^2$ scan area, along with the root mean square (RMS) roughness values measured for surface roughness. The RMS roughness of the perovskite thin film washed only with CB was measured as 51 nm, whereas the RMS roughness of the DCA-modified film was measured as 65 nm. Although the RMS value of the DCA-modified film has slightly increased, a noticeable increase in grain sizes is observed. As can be clearly seen from the AFM images, the DCA molecule has altered the surface properties and crystal sizes of the perovskite film, a finding that is also supported by XRD measurements.

Considering all these analyses, when triple-cation perovskite solar cells are prepared using the DCA molecule, improvements in open-circuit voltage (V_{OC}), short-circuit current density (J_{SC}), and fill factor (FF) values are expected. This enhancement can be attributed to a reduction in charge carrier recombination within both the bulk and interfacial regions of the triple-cation perovskite structure [33,34]. The hysteresis index (HI) of the device produced with DCA is negligible compared to the control device. The performance enhancements observed in DCA-modified PSCs can be attributed to the beneficial effects of this molecule on carrier lifetime and film quality. In the control cell, the lifetime of short-lived carriers (τ_1) is measured at 21.44 ns, and the lifetime of long-lived carriers (τ_2) is 94.03 ns, indicating a high recombination rate that limits efficiency compared to the DCA-modified device. In contrast, in the DCA-modified film, τ_1 increases to 44.43 ns and τ_2 to 208.53 ns. These results demonstrate that DCA molecules improve the crystal structure, allowing carriers to move without recombination for longer periods and thus increasing efficiency by extending carrier lifetime within the cell [35]. Longer carrier lifetimes enhance the mobility of free carriers while reducing recombination losses, contributing to an increase in J_{SC} and FF, as shown in Figure 6 and Table 2. Thanks to these structural effects, a larger apparent grain size and a highly crystalline film are obtained from DCA-modified films. This not only increases carrier lifetime but also limits ion mobility by passivating defects, reducing hysteresis [36,37]. The DCA-modified PSCs exhibited significant improvements in performance parameters such as J_{SC} , FF and PCE compared to the control devices. Under reverse scan, the DCA-modified cells achieved a J_{SC} of 22.9 mA/cm^2 (vs. 21.7 mA/cm^2 for control), FF of 64.1% (vs. 58.1% for control), and PCE of 14.6% (vs. 12.6% for control). Furthermore, the HI was significantly reduced to 0.0579 in DCA-modified cells (vs. 0.125 for control). [37]. Through enhancement of film structure and increased carrier lifetimes, the DCA molecule improves device performance by increasing both J_{SC} and FF.

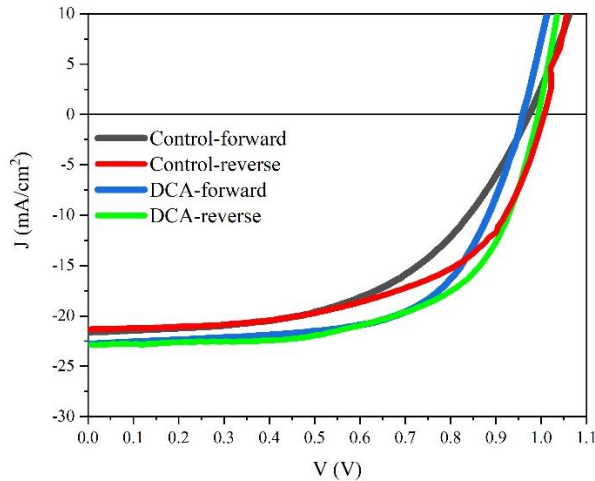


Figure 6. J-V curves obtained from devices fabricated with control and DCA-modified triple cation perovskite thin films under forward and reverse scan.

This study demonstrates that the addition of DCA additive to the anti-solvent during perovskite film formation can significantly enhance the structural and optoelectronic properties of PSCs. The DCA molecules affect crystallization kinetics, promoting crystal growth and enabling the production of films with lower defect densities. The perovskite films modified with DCA exhibited a substantial increase in PL intensity, indicating a significant suppression of non-radiative recombination in the perovskite layer and a reduction in trap state density. TRPL analyses revealed that DCA modification increased the carrier lifetime from $\tau_2=94.03$ ns to 208.53 ns; these results suggest that DCA enhances device performance by allowing charge carriers to move longer without recombination through defect passivation. The observed increase in carrier lifetimes and the reduction in non-radiative recombination losses contribute to a notable improvement in J_{SC} and FF while also mitigating hysteresis effects. The findings obtained from DCA modification can be considered a significant step towards developing high-efficiency PSCs.

4. Conclusion

Table 2. Electrical parameters obtained under forward and reverse scan from devices fabricated with control and DCA-modified triple cation PSCs.

	Scan direction	J_{sc} (mA/cm ²)	V_{oc} (mV)	FF (%)	PCE (%)	HI
Control	Forward	21.6	970	53.4	11.2	0.125
	Reverse	21.7	1000	58.1	12.6	
DCA	Forward	22.8	960	63.2	13.8	0.0579
	Reverse	22.9	995	64.1	14.6	

Acknowledgement

The authors gratefully acknowledge the financial support from the Presidency of the Republic of Turkey, Strategy and Budget Department (Project No: 16DPT002).

Author's Contributions

Adem Mutlu: Conceptualization, Methodology, Validation, Writing-original draft, Supervision, Writing-review and editing, Performed the analysis.

Sevdiye Başak Turgut: Collected data, Performed the analysis, Writing-review and editing.

Ethics

There are no ethical issues after the publication of this manuscript.

References

[1]. Khatoon vd., "Perovskite solar cell's efficiency, stability and scalability: A review", *Mater. Sci. Energy Technol.*, c. 6, ss. 437-459, 2023, doi: 10.1016/j.mset.2023.04.007.

[2]. N.-G. Park, "Perovskite solar cells: an emerging photovoltaic technology", *Mater. Today*, c. 18, sy 2, ss. 65-72, Mar. 2015, doi: 10.1016/j.mattod.2014.07.007.

[3]. B. Turedi vd., "Single-Crystal Perovskite Solar Cells Exhibit Close to Half A Millimeter Electron-Diffusion Length", *Adv. Mater.*, c. 34, sy 47, s. 2202390, Kas. 2022, doi: 10.1002/adma.202202390.

[4]. "best-research-cell-efficiencies chart, NREL". <https://www.nrel.gov/pv/assets/pdfs/best-research-cell-efficiencies.pdf>

[5]. H. Zhu vd., "Long-term operating stability in perovskite photovoltaics", *Nat. Rev. Mater.*, c. 8, sy 9, ss. 569-586, Eyl. 2023, doi: 10.1038/s41578-023-00582-w.

[6]. T. Ahmed Chowdhury, M. A. B. Zafar, M. S.-U. Islam, M. Shahinuzzaman, M. Aminul Islam, ve M. Uddin Khandaker, "Stability of perovskite solar cells: issues and prospects", *RSC Adv.*, c. 13, sy 3, ss. 1787-1810, 2023, doi: 10.1039/D2RA05903G.

[7]. G. Niu, W. Li, F. Meng, L. Wang, H. Dong, ve Y. Qiu, "Study on the stability of CH₃NH₃PbI₃ films and the effect of post-modification by aluminum oxide in all-solid-state hybrid solar cells", *J. Mater. Chem. A*, c. 2, sy 3, ss. 705-710, Ara. 2013, doi: 10.1039/C3TA13606J.

[8]. J. Bahadur, A. H. Ghahremani, S. Gupta, T. Druffel, M. K. Sunkara, ve K. Pal, "Enhanced moisture stability of MAPbI₃



- perovskite solar cells through Barium doping”, *Sol. Energy*, c. 190, ss. 396-404, Eyl. 2019, doi: 10.1016/j.solener.2019.08.033.
- [9]. “Understanding the Cubic Phase Stabilization and Crystallization Kinetics in Mixed Cations and Halides Perovskite Single Crystals | Journal of the American Chemical Society”. *J. Am. Chem. Soc.* 2017, 139, 9, 3320–3323, <https://pubs.acs.org/doi/10.1021/jacs.6b12432>.
- [10]. K. M. M. Salim vd., “Extended Absorption Window and Improved Stability of Cesium-Based Triple-Cation Perovskite Solar Cells Passivated with Perfluorinated Organics”, *ACS Energy Lett.*, Nis. 2018, doi: 10.1021/acsenerylett.8b00328.
- [11]. M. Saliba vd., “Cesium-containing triple cation perovskite solar cells: improved stability, reproducibility and high efficiency”, *Energy Environ. Sci.*, c. 9, sy 6, ss. 1989-1997, Haz. 2016, doi: 10.1039/C5EE03874J.
- [12]. W. Tan, A. R. Bowring, A. C. Meng, M. D. McGehee, ve P. C. McIntyre, “Thermal Stability of Mixed Cation Metal Halide Perovskites in Air”, *ACS Appl. Mater. Interfaces* 2018, 10, 6, 5485–5491, <https://pubs.acs.org/doi/full/10.1021/acsmi.7b15263>.
- [13]. M. M. Tavakoli vd., “Highly Efficient Flexible Perovskite Solar Cells with Antireflection and Self-Cleaning Nanostructures”, *ACS Nano* 2015, 9, 10, 10287–10295, <https://pubs.acs.org/doi/full/10.1021/acsnano.5b04284>.
- [14]. Q. Chen vd., “Planar Heterojunction Perovskite Solar Cells via Vapor-Assisted Solution Process”, *J. Am. Chem. Soc.* 2014, 136, 2, 622–625, <https://pubs.acs.org/doi/full/10.1021/ja411509g>.
- [15]. Y. Han vd., “Degradation observations of encapsulated planar CH₃NH₃PbI₃ perovskite solar cells at high temperatures and humidity”, *J. Mater. Chem. A*, c. 3, sy 15, ss. 8139-8147, Mar. 2015, doi: 10.1039/C5TA00358J.
- [16]. A. Mahapatra, D. Prochowicz, M. M. Tavakoli, S. Trivedi, P. Kumar, ve P. Yadav, “A review of aspects of additive engineering in perovskite solar cells”, *J. Mater. Chem. A*, c. 8, sy 1, ss. 27-54, Ara. 2019, doi: 10.1039/C9TA07657C.
- [17]. L. Han vd., “Environmental-Friendly Urea Additive Induced Large Perovskite Grains for High Performance Inverted Solar Cells”, doi: 10.1002/solr.201800054.
- [18]. N. K. Noel vd., “Enhanced Photoluminescence and Solar Cell Performance via Lewis Base Passivation of Organic–Inorganic Lead Halide Perovskites”, *ACS Nano* 2014, 8, 10, 9815–9821, <https://pubs.acs.org/doi/full/10.1021/nn5036476>.
- [19]. D. Xin, S. Tie, R. Yuan, X. Zheng, J. Zhu, ve W.-H. Zhang, “Defect Passivation in Hybrid Perovskite Solar Cells by Tailoring the Electron Density Distribution in Passivation Molecules”, *ACS Publ., Kas.* 2019, doi: 10.1021/acsmi.9b15166.
- [20]. J. Zhang vd., “Accelerated formation and improved performance of CH₃NH₃PbI₃-based perovskite solar cells via solvent coordination and anti-solvent extraction”, *J. Mater. Chem. A*, c. 5, sy 8, ss. 4190-4198, Şub. 2017, doi: 10.1039/C6TA10526B.
- [21]. K.-M. Lee vd., “Selection of anti-solvent and optimization of dropping volume for the preparation of large area sub-module perovskite solar cells”, *Sol. Energy Mater. Sol. Cells*, c. 172, ss. 368-375, Ara. 2017, doi: 10.1016/j.solmat.2017.08.010.
- [22]. D. Liu vd., “Efficient planar heterojunction perovskite solar cells with Li-doped compact TiO₂ layer”, *Nano Energy*, c. 31, ss. 462-468, Oca. 2017, doi: 10.1016/j.nanoen.2016.11.028.
- [23]. “Double-Halide Composition-Engineered SnO₂-Triple Cation Perovskite Solar Cells Demonstrating Outstanding Performance and Stability | ACS Applied Energy Materials”. *ACS Appl. Energy Mater.* 2020, 3, 9, 8595–8605, <https://pubs.acs.org/doi/10.1021/acsaem.0c01214>.
- [24]. “Managing grains and interfaces via ligand anchoring enables 22.3%-efficiency inverted perovskite solar cells | Nature Energy”. *Nature Energy* volume 5, pages131–140 (2020), https://www.nature.com/articles/s41560-019-0538-4?utm_source=acs&getft_integrator=acs.
- [25]. S.-G. Ko vd., “Effects of thiourea on the perovskite crystallization for fully printable solar cells”, *Sol. Energy Mater. Sol. Cells*, c. 196, ss. 105-110, Tem. 2019, doi: 10.1016/j.solmat.2019.03.045.
- [26]. Y. Liu vd., “Bridging Effects of Sulfur Anions at Titanium Oxide and Perovskite Interfaces on Interfacial Defect Passivation and Performance Enhancement of Perovskite Solar Cells”, *ACS Omega*, Ara. 2021, doi: 10.1021/acsomega.1c04685.
- [27]. T. Du vd., “Light-intensity and thickness dependent efficiency of planar perovskite solar cells: charge recombination versus extraction”, *J. Mater. Chem. C*, c. 8, sy 36, ss. 12648-12655, Eyl. 2020, doi: 10.1039/D0TC03390A.
- [28]. J. Jiang vd., “Carrier lifetime enhancement in halide perovskite via remote epitaxy”, *Nat. Commun.*, c. 10, sy 1, s. 4145, Eyl. 2019, doi: 10.1038/s41467-019-12056-1.
- [29]. J. Chang vd., “Crystallization and Orientation Modulation Enable Highly Efficient Doctor-Bladed Perovskite Solar Cells”, *Nano-Micro Lett.*, c. 15, sy 1, s. 164, Haz. 2023, doi: 10.1007/s40820-023-01138-x.
- [30]. “Reversible Photoinduced Phase Segregation and Origin of Long Carrier Lifetime in Mixed-Halide Perovskite Films”. *Volume30, Issue28, July 9, 2020, 2002622*, https://onlinelibrary.wiley.com/doi/epdf/10.1002/adfm.202002622?src=getfr&utm_source=acs&getft_integrator=acs.
- [31]. S. S. Mali, J. V. Patil, D. W. Park, Y. H. Jung, ve C. K. Hong, “Intrinsic and extrinsic stability of triple-cation perovskite solar cells through synergistic influence of organic additive”, *Cell Rep. Phys. Sci.*, c. 3, sy 6, s. 100906, Haz. 2022, doi: 10.1016/j.xcrp.2022.100906.
- [32]. S. Wang vd., “High-Performance Perovskite Solar Cells with Large Grain-Size obtained by using the Lewis Acid-Base Adduct of Thiourea”, doi: 10.1002/solr.201800034.
- [33]. D. W. deQuilettes vd., “Reduced recombination via tunable surface fields in perovskite thin films”, *Nat. Energy*, c. 9, sy 4, ss. 457-466, Nis. 2024, doi: 10.1038/s41560-024-01470-5.
- [34]. L. Fan vd., “Reducing charge-recombination losses in photovoltaic cells by spontaneous reconstruction of n/p homojunction in a monolithic perovskite film using black phosphorus nanosheets”, *Chem. Eng. J.*, c. 479, s. 147861, Oca. 2024, doi: 10.1016/j.cej.2023.147861.
- [35]. D. Shi vd., “Low trap-state density and long carrier diffusion in organolead trihalide perovskite single crystals”, *Science*, c. 347, sy 6221, ss. 519-522, Oca. 2015, doi: 10.1126/science.aaa2725.
- [36]. “Crystal Orientation and Grain Size: Do They Determine Optoelectronic Properties of MAPbI₃ Perovskite? | The Journal of Physical Chemistry Letters J. Phys. Chem. Lett. 2019, 10, 6010–6018, <https://pubs.acs.org/doi/10.1021/acs.jpcllett.9b02757>.
- [37]. “A multiscale ion diffusion framework sheds light on the diffusion–stability–hysteresis nexus in metal halide perovskites | Nature Materials”. *Nature Materials* volume 22, pages, 329–337 (2023), <https://www.nature.com/articles/s41563-023-01488-2>.